International Journal of Research in Engineering, Science and Management
Volume 4, Issue 7, July 2021
https://www.ijresm.com | ISSN (Online): 2581-5792

Dynamic Approach in Estimating Permeability in Tight Reservoir Rocks

Temidayo Boboye[1*], Oluwatoyin Akinsete[2]
[1]*Researcher, Department of Petroleum, University of Ibadan, Ibadan, Nigeria*
[2]*Senior Lecturer, Department of Petroleum Engineering, University of Ibadan, Ibadan, Nigeria*

***Abstract*: The impact of the permeability on ultra-tight porous media influences flow behaviour inside the media. The unconventional reservoir gas permeability significantly impacts rock property estimation crucial to unconventional resource development. The pressure decay approach estimates the permeability of unconventional rocks by evaluating the pressure difference in reservoirs. A representation of a mathematical model containing gas characteristics related to pressure was developed. When the minimum difference between the experimental pressure and the simulated pressure results stabilizes, the permeability estimation occurs. This study's approach estimated permeability from pulse pressure decay, using laboratory data by testing three gases that include Methane, Helium, and carbon dioxide. This new approach measures the slightest variation in the pressure decay response evaluation based on history matching. This method estimated permeability more accurately when compared with the Cui et al. (2009) analytical solution. The improved estimation of gas permeability in this study was due to the applicability of pressure-dependent gas properties and the entire pressure outcome's implementation to represent pressure decay dynamics. The sensitivity analysis shows that implementing the entire pressure outcome to represent the dynamics of pressure decay is significant in estimating permeability. In contrast, variation in porosity, Langmuir pressure, and Langmuir volume is less significant in the permeability estimation, making the pulse pressure decay approach for estimating permeability to be valid.**

***Keywords*: permeability, pulse pressure decay, pressure-dependent gas properties, transient approach, steady state approach.**

1. Introduction

The objectives of this research include Investigate the effects of various controlling factors on the determination of permeability. Also, to develop a comprehensive reservoir model simulation that gives an accurate determination of permeability by incorporating all essential controlling factors for an improved, efficient, and reliable approach for estimating permeability.

Permeability is an important intrinsic factor during gas production, and carbon sequestration. Permeability depends on the distribution of the pore size and its geometry. The importance of the accurate estimation of permeability in a porous media either for a multiphase or single-phase flow and the connection between the saturation, pressure cannot be overemphasized. In unconventional gas reservoirs, the matrix's pore size varies from 1nm and 100nm [28]. It enables permeability testing due to non-Darcy flow in the unconventional gas reservoir [13]. The movement of gas through the rock matrix is by either Darcy flow(advection) or diffusion. The complexity of unconventional reservoir gas movement makes it difficult to measure all the essential components contributing to optimized production fully. The complexity is evident by the co-existence of different flow regimes in the unconventional reservoir [19,20]. A potential inaccurate value of permeability occurred when conventional Darcy's flow is considered during permeability [12]. It is challenging to determine permeability in unconventional reservoirs by laboratory methods due to the inability to attain a steady-state flow; also, the low flow rates measured with high inaccuracy [18], [16]. There is a high potential risk of damage to tight rocks with the application of high volumes of fluids during the conventional measurement process [5].

Permeability evaluation is by both transient and steady-state approaches for tight rocks. Gas slippage describes the difference between liquid and gas [35]. The measurement of the permeability in unconventional reservoirs involves using a transient pulse-decay approach [17]. The pulse-decay method was initially used to measure granite's permeability, though the gas's fluid compressibility was neglected. [9] developed fully integrated analytical solutions that accounted for fluid compressibility storage effects relative to hydraulic head and pressure.

The gas compressibility is the ratio of the change in gas volume to the corresponding change in pressure at a constant temperature. The gas compressibility is higher with better compressibility storage effects compare to that of liquid. Ning et. al obtained permeability for fractured and un-fractured cores by history matching their pressure curves with an in-house built simulator. The operational complexity entails the exclusion of some intrinsic factors such as gas compressibility, use of large upstream and downstream reservoirs compares to the pore volume of the analytical solutions of Hsieh et al.'s work. The elimination of the operational complexity involves using an approximate analytical solution approach that yielded accurate results with smaller upstream and downstream volumes than

*Corresponding author: temidayoboboye@gmail.com

pore volume [15].

2. Background

A. Flow Mechanisms in Unconventional Reservoirs

The flow of gas in an unconventional reservoir is dependent on diffusion and Darcy flow. The gas will flow due to pressure differential. The flow of gas is mostly dependent on porosity and permeability in hydrocarbon reservoirs. Gas flow in unconventional reservoirs is through nanopore size with high velocity, which accounts for gas slippage effects. The quantification of the gas adsorption is by the amount of gas that is resident on the kerogen's surface, which changes pore pressure changes. Gas adsorption slows down transport processes and impacts the final pressure for a steady state. Gas compressibility influences the pressure difference.

B. Gas Compressibility

Isothermal gas compressibility determines the compressible properties of the reservoir. Gas is the most compressible element in porous media. Gas compressibility defines the relative change in the gas volume to the change in pressure at a constant temperature. The gas compressibility is expressed by,

$$C_g = \frac{-1}{V}\left(\frac{\partial V}{\partial P}\right) \quad (1)$$

The real gas compressibility expressed as:

$$C_g = \frac{1}{P} \quad (2)$$

The compressibility of a real gas written as:

$$C_g = \frac{1}{P} - \frac{1}{Z}\left(\frac{\partial z}{\partial P}\right)_T \quad (3)$$

By the real gas expression, it is evident that at low pressures, gas behaves as an ideal gas when the compressibility factor derivative to pressure sets to zero, and the gas compressibility conforms to an ideal gas. When pressures are low, gas compressibility is very high, resulting in a gas expansion to occupy a large volume at low pressure. At high pressures, gas compressibility reduces and results in liquid compressibility.

C. Desorption/Adsorption

Unconventional resources comprise of organic decay materials and kerogen. Gas in these resources can exist as free gas or absorbed gas (stored in pore networks). There is an increase in the release of absorbed gas as production increases with decreasing pressure. Langmuir isotherm adsorption describes desorbed gas, which accounts for a possible releasable amount of gas relative to the pressure in the pores.

$$C_e = \frac{q_L\ P}{P+P_L} \quad (4)$$

C_e is the adsorbed gas volume, P_L and q_L are Langmuir pressure and Volume in psi and m^3.

During the exploitation of an unconventional gas reservoir, the following parameters are of importance, which includes Langmuir parameter values, desorption pressure, and gas storage volume. Gas desorption plays a vital role in the unconventional reservoir gas production recovery. Unconventional rock absorbs a large amount of gas on its formation surface. Mainly methane absorbs on kerogen, and its absorption is quantified using Total Organic Content (TOC). More gas adsorption as production takes place with depleting pressure.

D. Experimental Layout

Before the experiment, the rock samples were shortened to about 2 inches with a diameter of 1 inch. A drying procedure was done for 24 hours and then put into aluminum foil (prevents interaction between sample and rubber jacket) placed in a rubber jacket (it prevents contact of the sample with confining gas). The experimental set-up replicates [37], with various valves ranging from 1 to 4. Gas flow into the sample is controlled by valve 1. The gas flow into the downstream reservoir is controlled by valve 2, while valves 3 and 4 controlled confining stress and axial load on the specimen from the triaxial cell.

The gas cylinder is embedded symmetrically with the two reservoirs on the left-hand side of the triaxial cell. The gas cylinder gives additional pressure to compensate for pressure in the upstream reservoir. The pressure pulsation is measured at the upstream and downstream reservoirs by two installed pressure transducers. Temperature is constant during the experiment, and the permeability is measured based on the pressure variations.

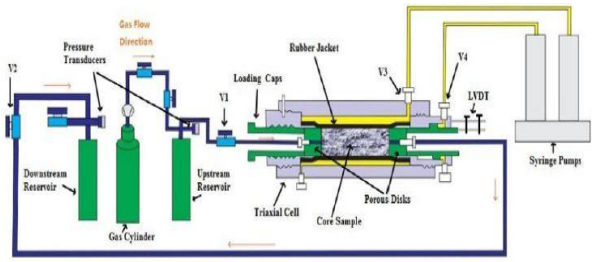

Fig. 1. Experimental setup of Wang et al.

E. Experimental Approach

The subsequent injection of three gases, namely methane, carbon dioxide, and helium, was used to study permeability measured at steady stress boundary conditions. The first cycle injection used helium, which is a non-sorbent gas. The helium gas was injected at a pressure of 14 psi into the upstream and downstream reservoirs until established in the downstream reservoir. However, the upstream had a continuous injection of helium gas until 31 psi. The gas injection introduction is by increasing the confining stress steadily to 1000 psi and a steady increase of axial load to 696 psi. The pressure of 31 psi in the upstream constituted the enabling force for the gas flow. The reservoir's confinement prevents interaction with downstream and triaxial cell by opening valve 1, which permits gas flow into the specimen. When the equilibrium is established in the

system, the experiment ends. From the pressure pulsation, the estimation of permeability occurred. A cyclic pattern established as the initial pressure ended. Values of pressures at upstream and downstream increased until equilibrium. The process involves six different pressure injection with helium. The same cyclic procedure is performed for methane and carbon dioxide for permeability measurements at the same confining and axial stresses.

F. Analytical Solution

Based on the previous research works [12] developed a modified analytical solution to the usual determination of permeability, resulting in an inaccurate permeability value because of adsorption term exclusion. The incorporation of the sorption term into the various corresponding governing equations gives a better result. Therefore, permeability is determined analytically by:

$$K = \frac{-s_1 \mu C_g L}{f_1 A\left(\frac{1}{V_u}+\frac{1}{V_d}\right)} \tag{5}$$

s_1 is the difference in upstream and downstream pressures slope on a semi-log. To fully replicate Cui et al.'s analytical solution, the slope of the pressure on semi-log is s_1. Equation 5 is valid for a minimal pressure difference between the upstream and downstream reservoirs at lower reservoir volume ratios.

$$f_1 = \frac{{\theta_1}^2}{a+b} \tag{6}$$

f_1 is the correction factor for mass flow by [23] model.

$$\tan\theta = \frac{(a+b)\theta}{\theta^2-ab} \tag{7}$$

$$a = \frac{V_p}{V_u}; \quad b = \frac{V_p}{V_d} \tag{8}$$

a and b denotes volume correlation of pore relative to downstream and upstream reservoir volumes. The storage capacity of the sample when methane and carbon dioxide are considered based on the adsorptive property as:

$$a = \frac{V_p\left(1+\frac{\phi_a}{\phi}\right)}{V_u} \quad b = \frac{V_p\left(1+\frac{\phi_a}{\phi}\right)}{V_d} \tag{9}$$

$$\phi_a = \frac{\rho_s (1-\phi) q_L P_L}{V_{std}\ C_g\ \rho (P_L+P)^2} \tag{10}$$

G. Mathematical Model Development

The model's development is from the governing equation with assumptions that intrinsic gas properties are pressure-dependent based on the experimental set-up of [38]. The governing equation comprises of gas compressibility storage effect, gas desorption or adsorption, and gas slippage effect. The comprehensive form model gives a non-linear equation that is solved by a numerical scheme of the finite difference approach. The model simulation is with MATLAB. The model is developed with the following assumptions: porosity is constant in time, single gas-phase flow, one dimensional linear flow, isothermal flow condition is present through the experiment, pressure dependent gas density, gas viscosity is constant, and the gas adsorption-desorption kinetics conforms with the Langmuir curve, which implies equilibrium for any reservoir pressure.

The mass conservation equation from the general form is,

$$\phi \frac{\partial \rho}{\partial t} = \frac{\partial}{\partial x}(\rho\, u) \tag{11}$$

Introduce adsorption term to the RHS of equation (11)

$$\phi \frac{\partial \rho}{\partial t} + (1-\phi)\frac{\partial C}{\partial t} = \frac{\partial}{\partial x}(\rho\, u) \tag{12}$$

where ϕ is porosity, ρ is gas density, C is the density adsorption per unit density of the rock.

Darcy Equation:

$$u = -\frac{k}{\mu}\frac{\partial p}{\partial x} \tag{13}$$

Adsorption:

Adsorption of the gas expression for gas volume per unit bulk volume of unconventional rock is.

$$C = \frac{\rho_s C_e}{V_{std}} \tag{14}$$

The expression for Volume of the gas adsorbed is:

$$C_e = \frac{q_L P}{P+P_L} \tag{15}$$

Put equation (15) into equation (14),

$$C = \frac{\rho_s}{V_{std}}\frac{q_L P}{P+P_L} \tag{16}$$

C is adsorption density per unit unconventional reservoir volume, q_L is Langmuir gas volume, C_e is adsorbed gas volume, P_L. is the pressure of Langmuir, V_{std} is the Volume of the sample under investigation.

Gas Compressibility:

The gas density is determined by,

$$\rho = \frac{P}{ZRT} \tag{17}$$

The gas compressibility expressed at isothermal temperature is:

$$C_g = \frac{1}{\rho}\left(\frac{\partial \rho}{\partial P}\right)_{.T.} \tag{18}$$

Re-arrange equation (18),

$$\rho\, C_g = \left(\frac{\partial \rho}{\partial P}\right)_T \tag{19}$$

An expression for the time derivative of accumulation is:

$$\frac{\partial \rho}{\partial t} = \frac{\partial \rho}{\partial P}\frac{\partial P}{\partial t} \tag{20}$$

Insert equation (13) into equation (12).

The complete model equation is given below, which is a non-linear variable because the gas properties are varying.

$$\phi \frac{\partial \rho}{\partial t} + (1-\phi)\frac{\partial C}{\partial t} = \frac{\partial}{\partial x}\left(\frac{k\rho}{\mu}\frac{\partial P}{\partial x}\right) \tag{21}$$

Initial and Boundary Conditions:

Initial Condition

The initial condition is explicitly expressed as the pressure at the downstream at the initial condition.

$$P(x, t=0) = P_d \quad for\ range\ 0 < r < L \tag{22}$$

Boundary Condition:

For boundary conditions, all equations depend on mass balance, and the change of the gas amount is equivalent to the amount of gas inflow or outflow.

In the upstream

$$P(x=0, t) = P_u \quad for\ any\ time\ t \geq 0 \tag{23}$$

At the downstream

$$P(x=L, t) = P_d \quad for\ any\ time\ t \geq 0 \tag{24}$$

Develop mass conservation equations upstream and downstream.

$$\frac{\rho KA}{\mu}\frac{dP}{dx}|_{r=0} = V_u \frac{d\rho_u}{dt} \quad for\ any\ time\ t > 0 \tag{25}$$

$$\frac{\rho KA}{\mu}\frac{dP}{dx}|_{r=L} = V_d \frac{d\rho_d}{dt} \quad for\ any\ time\ t > 0 \tag{26}$$

H. Numerical Simulation

$$\phi \frac{\partial \rho}{\partial t} + (1-\phi)\frac{\partial C}{\partial t} = \frac{\partial}{\partial x}\left(\frac{k\rho}{\mu}\frac{\partial P}{\partial x}\right) \tag{27}$$

Insert equation (17) into equation (27),

$$\frac{\phi}{RT}\frac{\partial\left(\frac{P}{Z}\right)}{\partial t} + (1-\phi)\frac{\partial C}{\partial t} = \frac{\partial}{\partial x}\left(\frac{k\rho}{\mu}\frac{\partial P}{\partial x}\right) \tag{28}$$

The numerical solution for the general model equation is given in equation (28).

The iteration step represents by r. Implementation of average harmonic estimation for the middle term in RHS of equation (29).

$$\frac{\phi}{RT}\frac{\left(\frac{P_i^{(r+1)}}{Z_i^{(r)}}\right)^{n+1} - \left(\frac{P}{Z}\right)_i^n}{\Delta t} + (1-\phi)\frac{C_i^{n+1\ (r)} - C_i^n}{\Delta t} = \left(\frac{k\rho}{\mu\Delta x^2}\right)_{i+\frac{1}{2}}^{n+1(r)} P_{i+1}^{n+1(r+1)} - \left[\left(\frac{k\rho}{\mu\Delta x^2}\right)_{i+\frac{1}{2}}^{n+1(r)} + \left(\frac{k\rho}{\mu\Delta x^2}\right)_{i-\frac{1}{2}}^{n+1(r)}\right] P_i^{n+1\ (r+1)} + \left(\frac{k\rho}{\mu\Delta x^2}\right)_{i-\frac{1}{2}}^{n+1(r)} P_{i-1}^{n+1\ (r+1)} \tag{29}$$

$$\left(\frac{k\rho}{\mu\Delta x^2}\right)_{i+\frac{1}{2}} = \frac{1}{\left(\frac{k\rho}{\mu\Delta x^2}\right)_{i+\frac{1}{2}}} = \frac{1}{2}\left[\frac{1}{\left(\frac{k\rho}{\mu\Delta x^2}\right)_i} + \frac{1}{\left(\frac{k\rho}{\mu\Delta x^2}\right)_{i+1}}\right] \tag{30}$$

$$\left(\frac{k\rho}{\mu\Delta x^2}\right)_{i-\frac{1}{2}} = \frac{1}{\left(\frac{k\rho}{\mu\Delta x^2}\right)_{i-\frac{1}{2}}} = \frac{1}{2}\left[\frac{1}{\left(\frac{k\rho}{\mu\Delta x^2}\right)_i} + \frac{1}{\left(\frac{k\rho}{\mu\Delta x^2}\right)_{i-1}}\right] \tag{31}$$

The numerical expression above is for $1 \leq i \leq N_x$. The number grid block is represented by N_x, which does not include the boundary grid block. The old-time level and new time level are denoted by N and $N+1$, respectively. i denotes the centre of the grid block. The upstream location is represented by $i = 1, i-1$, while the downstream location is $i = N_x, i+1$. Space and time steps are denoted respectively by Δx and Δt in the numerical simulation.

The Δx from this expression is:

$$\Delta x = \frac{L}{N_x+1} \tag{32}$$

From equation (32), L is the length of the sample (Grid block boundary from the left end to grid block boundary at the right end). The distance between the grid block center to center is equal, therefore:

$$\Delta x = \Delta_{x1} = \Delta_{x1} = \Delta_{x1} = \cdots = \Delta x_{N_x} = \frac{L}{N_x+1} \tag{33}$$

The values of upstream and downstream pressures at new time steps would be the inputs calculated from the numerical solution of the boundary conditions.

$$\frac{\rho\, KA}{\mu}\frac{P(1)^n - P_u^n}{\Delta x} = V_u \frac{\rho_u^{n+1} - \rho_u^n}{\Delta t} \tag{34}$$

$$\frac{\rho\, KA}{\mu}\frac{P(N_x)^n - P_d^n}{\Delta x} = V_d \frac{\rho_d^{n+1} - \rho_d^n}{\Delta t} \tag{35}$$

Constant Gas Properties Approach:

By making some modifications to the above model such that varying gas properties are kept constant, the general model for constant gas properties becomes [12]. The equation below estimates pressure as it varies along with the cylindrical sample.

$$\frac{\partial \rho}{\partial t} = \frac{k}{\mu C_g(\phi+(1-\phi)k_a)}\frac{\partial^2 P}{\partial x^2} \quad for\ 0 < x < L, at\ t > 0 \tag{36}$$

The initial condition gives:

$$P(r, t = 0) = P_d \quad for\ range\ 0 < r < L \tag{37}$$

The boundary conditions for the constant gas properties modelling are below.

$$P(r = 0, t) = P_u\ (t) \quad for\ any\ time\ t \geq 0 \tag{38}$$

$$P(r = L, t) = P_d\ (t) \quad for\ any\ time\ t \geq 0 \tag{39}$$

Mass conservation development based on the initial and boundary condition for the upstream and downstream are as follows:

$$\frac{KA}{\mu}\frac{dP}{dx}|_{r=0} = V_u\frac{d\rho_u}{dt} \quad for\ any\ time\ t > 0 \tag{40}$$

$$\frac{KA}{\mu}\frac{dP}{dx}|_{r=L} = V_d\frac{d\rho_d}{dt} \quad for\ any\ time\ t > 0 \tag{41}$$

3. Result and Discussion

Analysis of the sample permeability occurred using Carbon dioxide, Helium, and Methane. These gases have properties that are suitable for this study. Carbon dioxide and methane have sorption properties, unlike helium. The sorption and varying gas properties are instrumental in the sensitivity analysis of the model. The comparison of this method shows a better outcome than that of [12]. The simulated pressure and the corresponding permeability are the unknowns.

A. Results Presentation

1) Flushing Carbon dioxide through the sample

The adsorptive characteristics of carbon dioxide are higher relative to its high Langmuir volume and low Langmuir pressure. This characteristic of carbon dioxide is a distinctive feature against methane and helium gases. The excellent adsorptive characteristics of carbon dioxide account for a higher-pressure reduction rate after the stabilization of pressure. Table 1 shows the data used to estimate carbon dioxide to determine the pressure decay of permeability.

Figure 2 shows the Carbon Dioxide history match of the simulation and experimental for upstream and downstream.

Table 3 shows a summary of the outcomes of permeability. It is evident that permeability declines at the beginning with a steady recovery later, for increasing pressure rate. Although, this trend explains the large adsorption of carbon dioxide with a swelling effect in the matrix. The swelling impacted permeability reduction because the amount of carbon dioxide adsorbed has reduced with the increasing pressure of Langmuir sorption characteristics.

Table 2
Estimated permeability based on pressure values of carbon dioxide

Step	Pressure(psi)	Permeability (mD)	Objective function R (%)
1	21.900	1.480	2.400
2	109.120	0.900	0.380
3	223.350	0.620	0.210
4	339.520	0.550	0.120
5	468.400	0.590	0.069
6	584.190	0.660	0.045

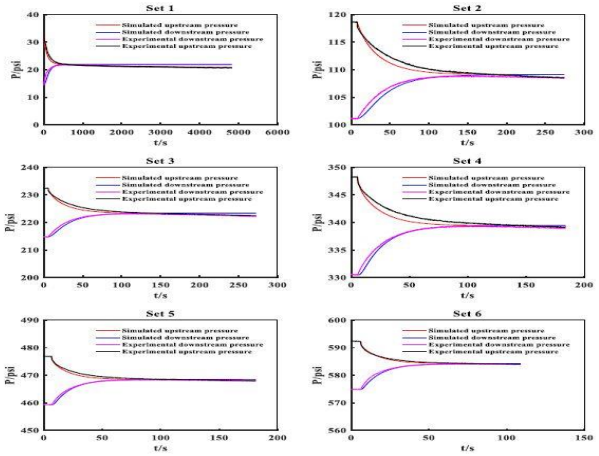

Fig. 2. Carbon dioxide history match of simulation, experimental for upstream and downstream

2) Flushing Methane through Sample

The simulated output of methane is presented from the inputs in Table 3. Adsorption is relevant to gas storage in the reservoir matrix—the impact of Langmuir parameters needed investigation for better understanding.

Table 1
Variables inputs used for Carbon dioxide

Variable	**Steps**					
	1	2	3	4	5	6
P_{ui} *(psi)*	32.20	118.64	231.85	348.23	476.88	592.30
P_{di} *(psi)*	14.70	101.15	214.85	330.48	459.31	574.93
μ *(Pa*s)* $* 10^{-5}$	1.484	1.490	1.501	1.519	1.548	1.588
C_g (Psi^{-1})	0.0460	0.00955	0.00491	0.00344	0.00273	0.00245
V_u $(m^3) * 10^{-5}$	2.998	2.998	2.998	2.998	2.998	2.998
$V_d(m^3)$	0.000018	0.000018	0.000018	0.000018	0.000018	0.000018
L (m)	0.0602	0.0602	0.0602	0.0602	0.0602	0.0602
A (m^2)	0.000507	0.000507	0.000507	0.000507	0.000507	0.000507
ϕ	0.12	0.12	0.12	0.12	0.12	0.12
P_e *(psi)*	21.90	109.12	223.35	339.52	468.46	584.19
q_L*(scf/ton)*	1170	1170	1170	1170	1170	1170
P_L *(psi)*	287.41	287.41	287.41	287.41	287.41	287.41

Table 3
Variables inputs used for methane

Variable	Steps					
	1	2	3	4	5	6
P_{ui} *(psi)*	32.05	141.79	256.51	370.05	482.65	610.04
P_{di} *(psi)*	14.71	124.29	238.92	352.54	464.96	592.59
μ *(Pa*s)*$*10^{-5}$	1.102	1.113	1.125	1.139	1.155	1.175
C_g (Psi^{-1})	0.0424	0.00759	0.00415	0.00288	0.00223	0.00178
V_u (m^3) $*10^{-5}$	2.998	2.998	2.998	2.998	2.998	2.998
$V_d(m^3)$ $*10^{-5}$	1.78	1.78	1.78	1.78	1.78	1.78
L (m)	0.0602	0.0602	0.0602	0.0602	0.0602	0.0602
A (m^2) $*10^{-4}$	5.07	5.07	5.07	5.07	5.07	5.07
ϕ	0.12	0.12	0.12	0.12	0.12	0.12
P_e *(psi)*	23.64	133.87	248.59	362.58	474.98	602.45
q_L*(scf/ton)*	393.3	393.3	393.3	393.3	393.3	393.3
P_L *(psi)*	380.24	380.24	380.24	380.24	380.24	380.24

Table 5
Variable input used for helium

Variable	Steps					
	1	2	3	4	5	6
P_{ui} *(psi)*	31.33	148.13	264.25	380.33	496.43	613.38
P_{di} *(psi)*	14.71	130.48	246.72	363.15	478.51	595.35
μ*(Pa.s)*$* 10^{-5}$	1.976	1.976	1.976	1.976	1.976	1.976
C_g (Psi^{-1})	0.0408	0.00708	0.00386	0.00265	0.00201	0.00162
$V_u(m^3)* 10^{-5}$	2.998	2.998	2.998	2.998	2.998	2.998
$V_d(m^3)* 10^{-5}$	1.78	1.78	1.78	1.78	1.78	1.78
L (m)	0.0602	0.0602	0.0602	0.0602	0.0602	0.0602
$A(m^2)* 10^{-4}$	5.07	5.07	5.07	5.07	5.07	5.07
ϕ	0.12	0.12	0.12	0.12	0.12	0.12
P_e *(psi)*	24.51	140.54	256.75	372.89	488.69	605.47

Figure 3 shows the set of history matched outcomes for methane gas flushing on the sample. The sample's storage capacity increased because of pressure reduction that occurred after the establishment of pressure equilibrium between pressures upstream and downstream [1]. The volume of gas adsorbed expressed by equation 15 is not affected by the established equilibrium of pressure from the history matched profile. Therefore, permeability estimation is based on excluding the equilibrium pressure in the pressure profile, which reduces the time for estimating permeability. In other words, the time required for the estimation of permeability reduces as the time for the establishment of equilibrium is not considered.

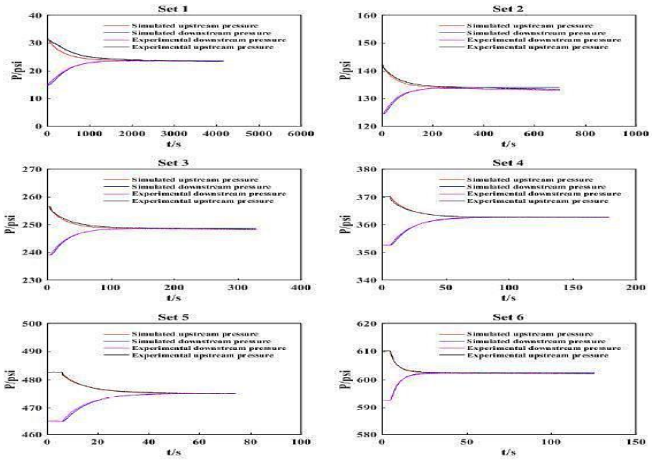

Fig. 3. Methane history match of simulation, experimental for upstream, and downstream

From table 4, the permeability estimation is based on the pressure with objective function for methane on the sample. Pressure increases from step 1 to step 6 at a range of 23.640 psi to 602.400 psi, which initially increased permeability at 23.640 mD to 0.870 mD. The progressive increment is related to impacts of sorption, swelling of matrix mechanisms. From this simulation, it is evident that permeability increases are dependent on pressure increases. However, changes in permeability are primarily impacted by pressure. Therefore, the sorption effect causes matrix swelling with minimal impact.

Table 4
Estimated permeability based on pressure values of methane

Steps	Pressure (psi)	Permeability (mD)	Objective function R (%)
1	23.640	0.250	1.900
2	133.870	0.310	0.260
3	248.590	0.360	0.098
4	362.580	0.420	0.030
5	474.980	0.540	0.026
6	602.410	0.870	0.022

3) Flushing Helium through Sample

The estimation of permeability with helium flushing on the sample, as shown in Table 5. The pressure at which permeability estimation occurs is the stabilization pressure.

Figure 5 depicts the history approximate of simulated outputs. The plots showed a consistent reproduce of experimental data plots, as seen in Table 7. The tolerance of the objective function is not exceeded. The distinctive characteristic of helium is its lack of sorption impacts, which results in increased permeability as a function of increased pressure. The pressure increases at a range of 24.510 psi to 605.470 Psi for a corresponding increase in permeability at range 0.870 mD to 2.910 mD.

Table 6
Estimated Permeability based on pressure values of helium

Step	Pressure (psi)	Permeability (mD)	Objective function R (%)
1	24.510	0.870	0.480
2	140.540	0.820	0.037
3	256.750	0.980	0.020
4	372.890	1.240	0.022
5	488.690	1.650	0.014
6	605.470	2.910	0.011

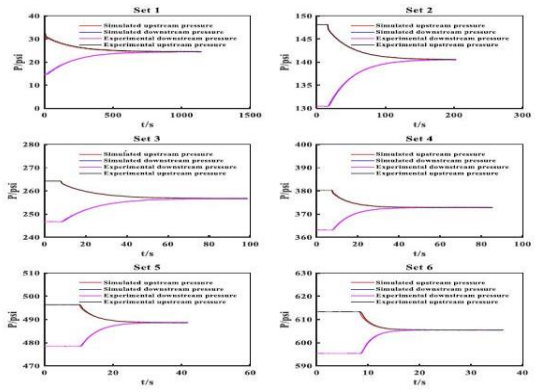

Fig. 4. Helium history match of simulation, experimental for upstream, and downstream

Variance in Permeability with Selected Gases:

From tables 3, 5, and 7, the variation in the permeabilities of carbon dioxide, Helium, and Methane as depicted by the plot of gases permeabilities versus pressure in Figure 10. It is evident that at a pressure of above 150 psi, helium has the highest permeability. The highest value of helium permeability distinguishes it from other studied gases as helium has negligible sorption effect, a least molecular diameter that enables accessibility of minute pores, and significant gas slippage effect. The sorption effect is dominant in carbon dioxide as permeability decreases above 200psi.

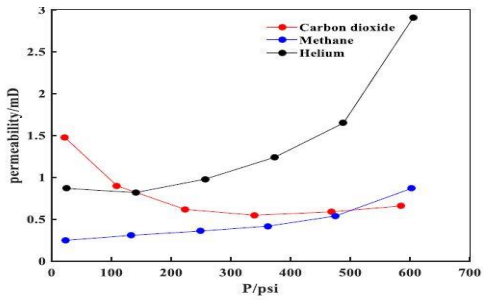

Fig. 5. Comparative permeability plots of studied gases as a function of pore pressure

Sensitivity Analysis:

A methodical approach to investigating intrinsic factors influencing the estimation of estimation. This study's approach centered on varying or constant gas properties as against the analytical approach of [12] to simulate history matching. Different permeability approaches were evaluated and compared based on their effects on estimated permeability. The study of the systematic investigation of intrinsic factors' influence on permeability estimation is for better understanding.

Results evaluation of permeability based on various models:

The three studied methods used in estimating the different gases' permeability under investigation and the results are comparatively weighed. The analytical solution approach from equation (5), termed an analytical solution. The numerical simulation based on equation (28), for varying gas properties approach, is called numerical solution 1, while the numerical solution with constant gas properties from equation (36) is called numerical solution 2.

Table 7
Numerical and analytical solutions for helium flushed sample for determining permeability

Step	Pressure (psi)	Analytical solution (mD)	Numerical solution 2 (mD)
1	24.51	0.72	0.82
2	140.54	0.84	0.82
3	256.75	1.00	0.97
4	372.89	1.28	1.23
5	488.69	1.80	1.62
6	605.47	3.02	2.87

Table 8
Numerical and analytical solutions for methane flushed sample for determining permeability

Step	Pressure (psi)	Analytical solution (mD)	Numerical solution 2 (mD)
1	23.64	0.19	0.24
2	133.87	0.28	0.3
3	248.59	0.31	0.36
4	362.58	0.42	0.41
5	474.98	0.45	0.53
6	602.45	0.62	0.85

Table 9
Numerical and analytical solutions for carbon dioxide flushed sample for determining permeability

Step	Pressure (psi)	Analytical solution (mD)	Numerical solution 2 (mD)
1	21.9	1.75	1.43
2	109.12	0.88	0.89
3	223.35	0.54	0.62
4	339.52	0.38	0.55
5	468.46	0.41	0.58
6	584.19	0.47	0.66

Figures 6 to 8 show comparative graphical representation of analytical solution and numerical solution 2 for the adsorptive gases under study, using data from Tables 7 to 9. From the graphs, it is evident that the disparity in analytical solution values and numerical solution 1 is subject to two reasons.

1. From the assumption that constant gas properties are pressure-dependent, the lower initial pressure or considerable differential pressure along the sample caused a notable error for the analytical solution. From figures 7 to 9, the numerical solutions 1 and 2 are approximately equal for high initial core pressure. A non-consistent permeability difference occurs for lower initial core pressure, although there is no effect on permeability outcome.
2. The numerical solution of permeability, estimation centred on the outline simulated and experimental pressures, and an analytical solution as determined from the late-time slope of pressure match. The

relative error impacted by either varied or constant gas properties is lesser than that of relative errors from the pressure match for the three gases. Therefore, the impact on permeability outcome occurs through the variation of experimental pressure data and simulated trends. Simulated and experimental pressure outlines best fit cannot by mere matching late-time slopes alone. Convolution of flow mechanisms in adsorptive gases exhibits higher relative error than gas without the adsorptive feature (Helium) for varied gas properties.

From the two established reasons above, it is evident that the second reason significantly influenced the permeability results estimation. Permeability estimation is realistic with a history matching approach. A systematic approach uses varying gas properties at the initial pressure step but applying constant gas properties give more accurate results as pressure increases.

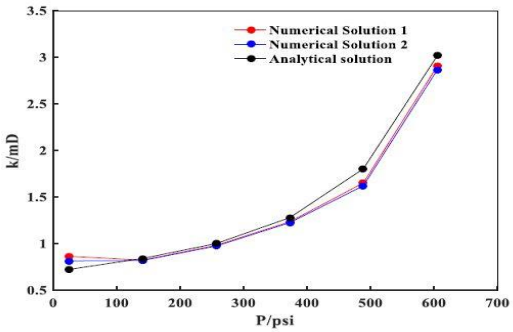

Fig. 6. Plot of permeability versus pressure for helium to compare various methods of permeability estimation

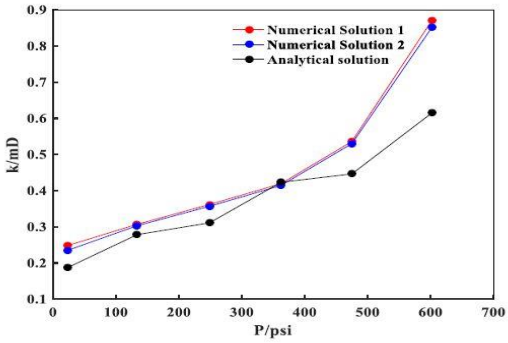

Fig. 7. Plot of permeability versus pressure for methane to compare various methods of permeability estimation

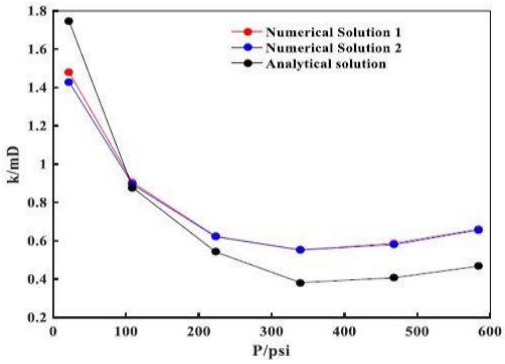

Fig. 8. Plot of permeability versus pressure for carbon dioxide to compare various methods of permeability estimation

Sensitivity of Differential Pressure to Porosity:

Using values from Table 2 with a constant permeability of 0.66 mD, and varying values of porosity in succession of 0.001, 0.01, 0.05, 0.08, 0.12, and 0.15. Figure 9 shows pressure plots for varying porosities. Varying porosity cannot influence permeability estimation outcomes based on experimental pressure difference outcomes. This assertion negates the work of [7] relative to the established permeability-porosity dependency. As porosity declines from the highest selected porosity value of 0.15 to the lowest value 0.001, this should cause a significant decrease in permeability. Therefore, different samples of different porosities will yield different results for differential pressure, then permeability estimation varies.

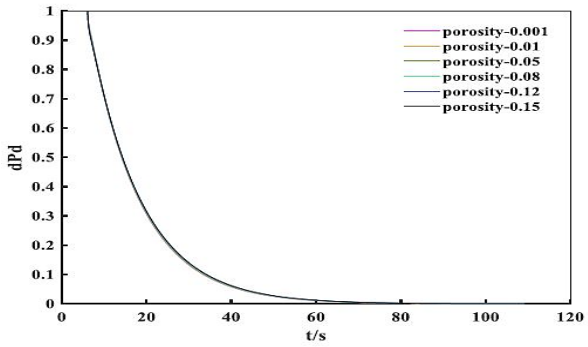

Fig. 9. Plot of differential pressure versus time for varying porosity values

Sensitivity of Differential Pressure to Gas Compressibility:

The differential pressure for various gases with reference to varying gas compressibility. The highest gas compressibility shows a significant effect on the permeability. This effect is prevalent even with a small pressure difference, and gas compressibility has a more significant effect on permeability estimation.

Sensitivity of Differential Pressure to Langmuir Pressure and Langmuir Volume:

Using the values from Table 2 with systematic values of Langmuir pressure and Langmuir volume with differential pressure to study these effects on the estimation of permeability. The investigation is with Langmuir pressure ranging from $100\,psi$ to $450\,psi$ and Langmuir volume ranging from $800\ scf/ton$ to $1300\ scf/ton$. Figures 10 and 11 show that curves of different Langmuir pressures or Langmuir volumes merge into a single curve. Estimated permeability changes a little for different values of Langmuir pressures or Langmuir volumes. The estimated permeability is accurate because varying Langmuir pressures and/or Langmuir volumes have a lesser impact.

With an increasing amount of gas, the corresponding pore pressure increases. The adsorptive characteristics of carbon dioxide are higher relative to its high Langmuir volume and low Langmuir pressure than that of Helium and Methane. The high Langmuir Volume and low Langmuir pressure would impact the analytical solution, thereby giving a less accurate permeability estimation.

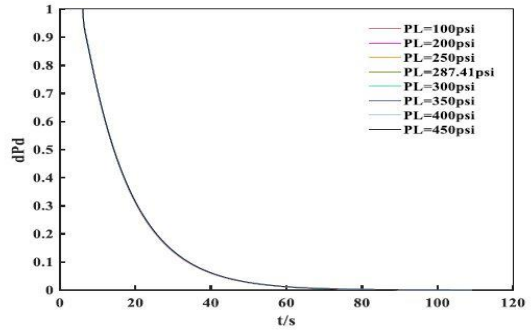

Fig. 10. Differential Pressure for various Langmuir pressures

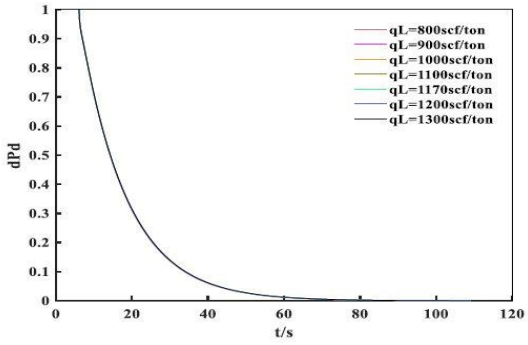

Fig. 11. Differential pressures for various Langmuir volumes

4. Conclusion

The outcomes show a related trend of permeability transformation, but with enhanced permeability outcomes as against analytical solutions. The enhanced permeability is related to the two-stage approach of constant gas properties for an analytical solution. An analytical solution of permeability acquired from simulation and experimental pressure outlines. The approach in this study is using history matching of simulated and experimental pressure outlines. From this study, the following assertions exist:

1. With a reduction in the effective stress, permeability estimation with helium increases with increasing pressure. Different adsorptive gases depict different permeability responses. Permeability increases as an effective stress decrease for methane gas are higher than matrix swelling caused by sorption induction. Carbon dioxide exhibits two different patterns such that with dominant sorption effect, permeability reduces, but as effective stress reduces, then permeability begins to increase. For pressure below 110 psi, carbon dioxide is the highest permeability, but at above 150 psi, helium is the highest permeability.
2. Based on the initial approach variance, there is no effect on permeability, even with a higher pressure. Even at low pressure, the same trend occurred. The variance between pressure along the sample for the three gases at all pressure steps for gas properties is little or negligible.
3. Based on the next approach variance, there is a more significant influence on permeability. The history matching approach gives a better estimation of permeability as against pressure outlines of simulated and experimental.
4. The systematic investigation of the effects of variations of porosity, gas compressibility, Langmuir pressure, and Langmuir volume indicated that estimated permeability was based on the changing values of the intrinsic factors.

References

[1] Aljamaan, H., Alnoaimi, K., Kovscek, A.R. "In-Depth Experimental Investigation of Shale Physical and Transport Properties," 2013.
[2] Alnoaimi, K.R. and A.R. Kovscek. " Experimental and numerical analysis of gas transport in shale including the role of sorption," *SPE Annu. Tech. Conf. Exhib. SPE 166375*. 2013.
[3] Aljamaan, H., Alnoaimi, K., Kovscek, A.R. "In-Depth Experimental Investigation of Shale Physical and Transport Properties." 2013.
[4] Alnoaimi, K.R. and A.R. Kovscek. " Experimental and numerical analysis of gas transport in shale including the role of sorption. ." *SPE Annu. Tech. Conf. Exhib. SPE 166375*. 2013.
[5] Amaefule, J.O., et al. "Laboratory determination of effective liquid permeability in low-quality reservoir rocks by the pulse decay technique." *SPE California Regional Meeting, 2-4 April, Oakland, California*.1986.
[6] American Petroleum Institute, API. "Recommended Practices for Core Analysis." *American Petroleum Institute (API)*, 1998.
[7] Berg, R.R. "Method For Determining Permeability From Reservoir Rock Properties." 1970.
[8] Beskok, A and G. Em Karniadakis. "A model for flows in channels, pipes, and ducts at micro and nano scales." *Microscale ThermoPhysical Engineering*, 3.1, 1999.
[9] Brace, W.F, J.B Walsh and W.T Frangos. "Permeability of granite under high pressure." *Journal geophysics Research and Space Physics*,73, pp 2225-2236, 1968.
[10] Cipolla, C.L. and E.P. Lolon. "Reservoir Modelling in Shale Gas Reservoirs.", 2010.
[11] Civan, F., C. S. Rai and C. H. Sondergeld. " Shale-gas permeability and diffusivity inferred by the improved formulation of relevant retention and transport mechanisms. Transport in Porous Media," 2011.
[12] Cui, X., A.M.M. Bustin and R.M. Bustin. "Measurements of gas permeability and diffusivity of tight reservoir rocks: Different approaches and their applications. ." *Geofluids* , 9 ,208–223, 2009.
[13] Darabi, H., A. Ettehad and F. Javadpour. "Gas flow in ultra-tight shale strata." *Journal of Fluid Mechanics*, 710 , 641-658, 2012.
[14] Darcy, H. Les fontaines publiques de la ville de Dijon. Paris: Dalmont ,1856.
[15] Dicker, A.I and R.M Smits. "A Pratical approachfor determining permeability from laboratory pressure-pulse decay measurements." *SPE*, 1988.
[16] Finsterle, S. and P. Persoff. "Determining permeability of tight rock samples using inverse modeling." *Water Resources Research* 33, pp. 1803–1811, 1997.
[17] Han, G, et al. "Differneces in Performance of Models for Heterogeneous Cores during Pulse Decay Tests." *Applied Science, 3206*, 9, 2019.
[18] Hsieh, P.A., et al. "A transient laboratory method for determining the hydraulic properties of "tight" rocks-I." *Int. J. Rock Mech. Min. Sci. Geomech. Abstr.* 18, 245-252, 1981.
[19] Javadpour. "Nanopores and apparent permeability of gas flow in mudrocks (shales and siltstone)." *Journal of Canadian Petroleum Technology* ,48.8, pp. 16-21, 2009.
[20] Javadpour, F., D. Fisher and M. Unsworth. "Nanoscale Gas Flow in Shale Gas Sediments." *Journal of Canadian Petroleum Technology* ,46, 2007.
[21] Javadpour, F.,. "Nanopores and apparent permeability of gas flow in mudrocks (shales and siltstone)." *Journal of Canadian Petroleum Technology.* , pp. 16-21, 2009.
[22] Jia, B., J.-S. Tsau and R. Barati. "Different Flow Behaviorsnof Low-Pressure and High-Pressure Carbon Dioxide in Shales." *SPE Journal* ,23, pp 1452-1468, 2018.
[23] Jones, S.C. "A Technique for Faster Pulse-Decay Permeability Measurements in Tight Rocks.", 12, pp. 19-26, 1997.
[24] Kamath, J., R. Boyer and F. Nakagwa. "Characterization of Core Scale Heterogeneities using Laboratory Pressure Transients." *SPE Formation Evaluation*, 7, pp. 219-227, 1992.
[25] Knudsen, M. *Ann. Phys., Lpz* 28, pp 75-130, 1909.
[26] Langmuir, I. "The constitution and fundamental properties of solids and liquids," *Journal of American Chemical Society*, 38 , 11, 1916.

[27] Liehui, Z. "Well Production Performance Analysis for Shale Gas Reservoirs." *Develoments in Petroleum Science, Elsevier*, 66, 2019.
[28] Loucks, Robert G., et al. “Morphology, genesis, and distribution of nanometer-scale pores in siliceous mudstones of the Mississippian Barenett Shale.” *Journal of Sedeimentary Research* ,79, 12, pp. 848-861, 2009.
[29] Michel, et al. "Parametric Investigation of Shale Gas Production Considering Nano-Scale Pore Size Distribution, Formation Factor, and Non-Darcy Flow Mechanisms.", 2011.
[30] Moghanloo, R. G., F. Javadpour and D. Davudou. "Contibution of Methane Molecule Diffusion in Kerogen to Gas-in-Place and Production. ." *SPE Western Regional & AAPG Pacific Section Meeting, Joint Technical Conference*, 2013.
[31] Ning, X. The measurement of Matrix and fracture Properties in Naturally Fracture Low Permeability Cores Using a Pressure Pulse Method. Texas, 20 June 1992.
[32] Peaceman, D.W. "Fundamentals of Numerical Reservoir Simulation." 6, 1977.
[33] Sakhaee-Pour, A. and S. Bryant. "Gas Permeability of Shale." *Society of Petroleum Engineers* , 2012.
[34] Swanson, B.F. "A simple correlation betweem permeability and mercury pressure curve." *Journal of Petroleum Technology*, 27, pp. 2498-2504, 1981.
[35] Tanikawa, W and T Shimamoto. "Correction to "comparison of Klinkenberg-corrected gas pemeability and wate pemeability in sdimntary rocks"." *International Journal of Rock Mechanics and Mining Science*, 46, pp. 1394-1395 (2009.
[36] U.S Energy Information Agency, EIA. U.S Energy Information Agency, EIA.,(2019) Annual Energy Outlook, 2019.
[37] Wang, H. and M Marongiu-Porcu. "Impact of Shale-gas Apparent Permeability on Production: Combined Effects of Non-Darcy Flow/Gas-Slippage, Desoprtion, and Geomechanics." *Society of Petroleume Engineers*, 2015.
[38] Wang, Y., S. Liu and D. Elsworth. " Laboratory investigations of gas flow behaviors in tight anthracite and evaluation of different pulse-decay methods on permeability estimation." *Int. J. Coal Geol.*, 149, pp. 118-128, 2015.
[39] Xu, B., M. Haghighi and D. Cooke. "Production Data Analysis in Eagle Ford Shale gas Reservoir." *Society of Petroleum Engineer*, 2012.
[40] Ziarani, A. S. and R. Aguilera. "Transp Porous Media.", 2012.